JOURNAL OF APPLIED ELECTROCHEMISTRY **29** (1999) 301–311.

Nickel ferrite as inert anodes in aluminium electrolysis: Part II Material performance and long-term testing

E. OLSEN[1*] and J. THONSTAD[2]

[1]*SINTEF Materials Technology, Electrolysis Group, N-7034 Trondheim, Norway;* [2]*Department of Electrochemistry, Norwegian University of Science and Technology, Norway*
*(*author for correspondence, e-mail: espen.olsen@matek.sintef.no)*

Received 23 May 1997; revised 20 April 1998

The behaviour of three different compositions based on nickel ferrite–nickel oxide–copper cermets was investigated as anode materials in laboratory electrolysis tests for 50 h in a conventional cryolite-based electrolyte. The corrosion of the anodes was assumed to be mass transfer controlled and the transfer of impurities into the electrolyte and subsequently into the cathodically deposited metal was studied. The results indicate that the materials corroded in a controlled manner. Mass transfer coefficients of species from the anode to the electrolyte were of the order of $10^{-4}\,m\,s^{-1}$ while the mass transfer coefficients for transfer of the species from the electrolyte into the deposited metal were of the order of $10^{-6}\,m\,s^{-1}$. Nickel exhibited significantly lower mass transfer coefficients than those of iron and copper. The extrapolated corrosion rates of the anode ranged 1.2–2.0 cm year^{-1}, which is acceptable from an industrial perspective. The contamination of the deposited aluminium with respect to Ni and Cu was, however, too high to meet current specifications for commercial grade metal. Post-electrolysis examination of the anodes showed that a reaction layer of approximately 50 μm thickness was formed on the anodes. This layer did not contain any metal grains and seemed to prevent preferential corrosion of the metal phase in the underlying cermet.

Keywords: *aluminium, cermet, electrode, electrolysis, inert,* $NiFe_2O_4$

1. Introduction

As outlined in Part I [10], attempts have been made to replace the present day consumable carbon anode used in the Hall–Heroult process with an inert anode, the cell reaction then being,

$$Al_2O_3 = 2Al + \tfrac{3}{2}O_2 \qquad (1)$$

The first reported work in this field is due to Belyaev and Studentsov [32, 33] who examined various oxides and ferrites as candidate materials for inert anodes. A number of materials were found to have a very low solubility in cryolitic melts. Alusuisse investigated and patented a range of materials based on tin oxide (SnO_2) for use as inert anodes. Since then, a number of attempts have been made to develop an inert, oxygen-evolving anode material for aluminium electrowinning, based on a number of materials. A considerable number of patents have also been issued [1–3, 21–25]. Supported by US Department of Energy, Aluminum Company of America (Alcoa) conducted significant work on the use of ferrites [4]. They developed a new cermet material consisting of a nickel ferrite–nickel oxide substrate containing Cu as a metal phase to provide acceptable electrical conductivity. Excess NiO was added to ensure an activity coefficient of unity for nickel oxide, as this phase has a significantly lower solubility in cryolite than Fe_2O_3 [4]. The work was continued by Battelle Pacific Northwest Laboratories, but they were not able to reproduce the best results obtained by Alcoa [5–9]. Important work has also been published by a number of authors such as Sadoway [26, 32], Hryn and Sadoway [29], Windish [6], Zöllner [30] and Sekhar *et al.* [31].

In the present study, we have conducted electrolysis tests for 50 h. In the preceding paper [10] we found that tests which lasted for 4 h were too short to achieve steady state with respect to the distribution of impurity species in the bath and in the deposited aluminium metal. In the ceramic phase, the materials contained varying amounts of NiO with respect to $NiFe_2O_4$. The three compositions contained 0, 17 and 23 wt% excess NiO respectively. These tests have enabled us to discuss the transfer of impurities originating from the anode material, dissolving from the anode surface into the electrolyte and further being reduced and entering into the deposited aluminium at the cathode. A simple model based on mass transfer control of impurities was used to calculate mass transfer coefficients for the various impurities at both electrode–electrolyte interfaces. Corrosion rates were calculated based on the contamination of the cathode metal by species originating from the anode. The used anodes were investigated extensively by SEM and X-ray microanalysis (XRMA) techniques to study their performance.

2. Objective

This work set out to study three aspects:

(1) To test the specimens prepared with organic solvents and dispersants in a scaled-up cell compared to the one used in short-term experiments reported in Part 1 [10]. Tests over a longer period of time were planned in order to evaluate better the performance of the different compositions.

(2) To study the effect of varying NiO content in the cermets on the performance of the material, as well as the contamination of anode species in the electrolyte and the deposited aluminium.

(3) To further develop a model proposed by Evans and Keller [15]. This model describes the mass transfer of corrosion products from the oxide anode surface, through the electrolyte with subsequent reduction into the deposited aluminium. The model describes the process at steady state. A basic mathematical treatment could also help to test this model in the non-steady state when the electrolyte is not saturated with contaminating species.

3. Theory

A cermet material is subject to two different dissolution mechanisms when anodically polarized in the electrolyte. The metallic phase may undergo electrochemical anodic dissolution, while the ceramic matrix, being in the oxidized, electrochemically stable state, will show chemical dissolution. It has been shown by Tarcy [12] that, in a similar nickel ferrite cermet with a nickel metallic phase, the nickel dissolved electrochemically, leaving open pores allowing the electrolyte to penetrate into the anode. When nickel was replaced by a Cu/Ni alloy as the metal phase, this did not occur. This alloy does not form a continuous network, and the electrochemical process should stop when all metal particles exposed to the electrolyte have dissolved. From then on, the process will be controlled by chemical dissolution of the oxide phase with only a limited number of alloy particles being exposed to the electrolyte as the interface recedes with the slowly dissolving ceramic phase. Formation of a fairly stable copper oxide layer on the metal may also inhibit the anodic dissolution process. Tests performed by Hall with solid copper electrodes showed that copper forms an oxide layer on the surface [13]. However, XRD measurements of cermet anode surfaces did not show any copper oxides to be present on the surface layer [14]. The process which governs the dissolution and transport of the alloy species from the cermet surfaces might therefore be different from chemical dissolution.

Aluminium has finite solubility in molten cryolite, and will attack the oxides on the surface of an unpolarized anode. On an oxygen-evolving anode, however, dissolved aluminum is prevented from getting into direct contact with the anode substrate.

As mentioned above, the model proposed by Evans and Keller assumes that the corrosion mechanism of a ceramic anode material is mass transport controlled [15]. Since these authors only treated the steady-state case, mathematical considerations to include the non-steady state are presented below.

The dissolved anode species are transported to the cathode where they are deposited cathodically or react with aluminium in a red-ox reaction,

$$\mathrm{Al} + \tfrac{3}{n}\mathrm{M}^{n+} = \mathrm{Al}^{3+} + \tfrac{3}{n}\mathrm{M} \qquad (2)$$

Assuming mass transfer control and a linear first-order reaction with no initial contamination of the electrolyte, the diffusion equation describing the dissolution of oxide species from the anode and the transfer to the cathode is:

$$(c_{\mathrm{sat}} - c(t))k_{\mathrm{an}}A_{\mathrm{a}} - c(t)k_{\mathrm{cal}}A_{\mathrm{m}} = V\frac{\partial c(t)}{\partial t} \qquad (3)$$

where $c(t)$ is the time-dependent concentration of species in the electrolyte (mol m^{-3}), c_{sat} the saturation concentration of the species (mol m^{-3}), k_{an} the mass transfer coefficient anode-electrolyte of the species (m s^{-1}), k_{cat} the mass transfer coefficient electrolyte-metal pad (m s^{-1}), A_{a} the surface area of anode (m^2), A_{m} the surface area of cathode (m^2) and V the volume of electrolyte (m^3).

The solution of Equation 3 for this problem is given by

$$c(t) = \frac{k_{\mathrm{an}}c_{\mathrm{sat}}A_{\mathrm{a}}}{k_{\mathrm{cat}}A_{\mathrm{m}} + k_{\mathrm{an}}A_{\mathrm{a}}}\left(1 - \exp\left(\frac{-(k_{\mathrm{cat}}A_{\mathrm{m}} + k_{\mathrm{an}}A_{\mathrm{a}})t}{V}\right)\right) \qquad (4)$$

which can be simplified to:

$$c(t) = B(1 - \exp(-1/\tau)) \qquad (5)$$

The overall rate of reaction 2 is believed to be mass transfer controlled, and is accommodated in the total mass transfer equation for this system via the cathodic mass transfer coefficient k_{cat}. This alloying process takes place in a rather stagnant layer at the electrolyte/cathode interface and k_{cat} is assumed to be much smaller than the coefficient for anode dissolution, k_{an}, if both reactions are governed by mass transport [15]. On the other hand, if a chemical reaction occurs at the anode surface prior to dissolution and subsequent mass transfer, this might not be the case. If we assume that $k_{\mathrm{an}} \gg k_{\mathrm{cat}}$ and $A_{\mathrm{m}} \approx A_{\mathrm{a}}$ constant B can be set equal to c_{sat}. The time constant, τ, is then expressed by:

$$\tau = \frac{V}{k_{\mathrm{cat}}A_{\mathrm{m}} + k_{\mathrm{an}}A_{\mathrm{a}}} = \frac{V}{(k_{\mathrm{an}} + k_{\mathrm{cat}})A} \qquad (6)$$

This gives an equation for species dissolution under mass transport control with zero initial concentration of that species:

$$c(t) \approx c_{\mathrm{sat}}(1 - \exp(-1/\tau)) \qquad (7)$$

For this equation to be applicable in a real electrolytic cell, it is necessary to incorporate the initial concentrations of impurities in the electrolyte. As the

final, steady-state concentration in the electrolyte is dependent not only on the dissolution of the anode material, but also on the transfer of species into the metal, it is not strictly correct to use c_{sat}, that is the saturation concentration of the species in the electrolyte, as the steady-state value. The steady-state concentration in the electrolyte will be reached when the dissolution of the anode material occurs at the same rate as the anode components are removed from the electrolyte, either by dissolution into the metal or by loss to the vapour phase. The removal of species via the vapour phase will not be discussed here as the transfer of impurities to the vapour phase is not well understood. For most components only a small fraction escapes via the vapour phase.

The steady-state concentration in the electrolyte can be substituted by a value c_∞. Equation 8 describes, in general terms, the concentration vs time relationship for a dissolving species

$$\frac{c(t) - c_0}{c_\infty - c_0} = 1 - \exp(-1/\tau) \tag{8}$$

with a steady-state concentration of c_∞ and an initial concentration c_0, which transforms into Equation 9.

$$c(t) = c_\infty - (c_\infty - c_0)\exp(-1/\tau) \tag{9}$$

In Equation 9. c_∞ denotes the concentration at steady state and c_0 denotes the initial content of the impurity in the electrolyte. This equation can be used to determine the mass transfer coefficients in the system by fitting of the curves to suit the measured data.

The mass transfer coefficients can be calculated using Equations 6, 7 and 9. The c_∞ value can be used as a good estimate for c_{sat} if $k_{an} \gg k_{cat}$. This implies that if the model and the assumptions made are correct, the steady-state concentration in the electrolyte of species dissolving from the anode should be close to saturation.

When the system has reached steady state, the incorporation of anode species into the cathode will occur at a constant rate as the amount dissolving at the anode will be equal to that entering the aluminium cathode. This is described by Equation 10.

$$J = k_{an}(c_{sat} - c_\infty)A_a = k_{cat}c_\infty A_m \tag{10}$$

This is the model first proposed by Evans and Keller [15].

4. Experimental

The cell used in the 50-h electrolysis tests is sketched in Fig. 1 [11]. It consisted of a graphite crucible lined with a thick-walled sintered alumina tube. The inner diameter of the tube was 100 mm. In the bottom of the cell was placed a rectangular piece (5 × 5 cm) of TiB_2–graphite composite (95% TiB_2, 5% C, Great Lakes Carbon) to serve as cathode (all compositions are given in wt%, unless otherwise stated). The rest of the cell bottom was insulated with a disc of 10 mm thick sintered alumina. The crucible and the TiB_2

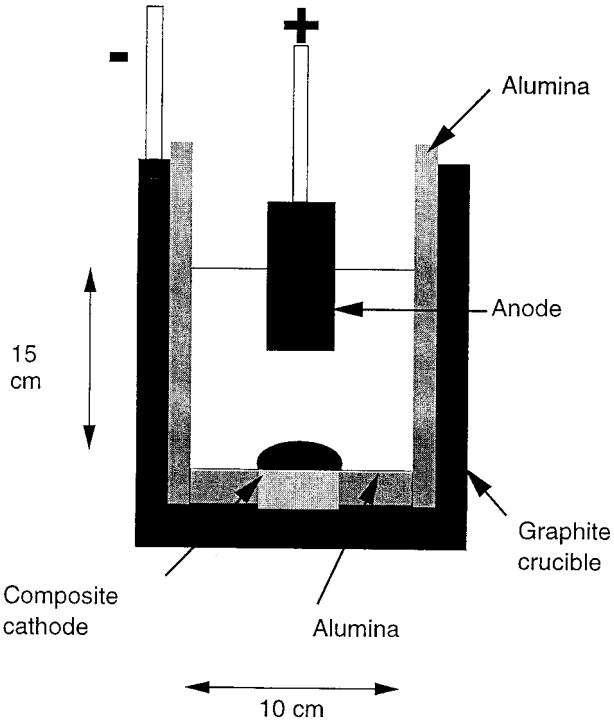

Fig. 1. Electrochemical cell used in the 50-h experiments.

composite cathode were polarized cathodically through a 6 mm Inconel rod. The anodic current was provided through a similar Inconel rod attached to the anode with Cu-based cement. The anode current lead was protected from corrosion with a sintered alumina tube. A cylindrical cermet anode (8 cm high, 4 cm diameter, immersion depth 5 cm) was used.

The cell contained a total of 2300 g electrolyte of CR 2.2 (NaF/AlF_3 molar ratio). The electrolyte contained 5 wt% CaF_2 (as against 10 wt% in Part I of this paper [10]) and the alumina concentration was kept close to saturation (8 wt%) throughout the tests. The temperature was 960 °C. In order to ensure that the deposited aluminium would wet the cathode from the start of the experiment, 9 g of high purity A1 was placed on top of the cathode prior to electrolysis.

To determine the concentration of anode constituents in the melt during the tests, electrolyte samples were taken frequently by rapid freezing onto a graphite cylinder which was quickly immersed into the electrolyte. Changes in the concentration in the initial phase of the test were considered important in the sense that it could be used to determine the mass transfer coefficient of the various species from the anode into the electrolyte. Samples were, therefore, taken at 5-min intervals for the first 30 min of the tests, then every 10 min for the following 30 min. Preliminary tests had shown that the electrolyte reached constant concentration of species originating from the anode after about 60 min. Later in the tests, the samples were taken at random intervals associated with metal sampling. The electrolyte samples were analysed using XRF spectroscopy. The precision of the method is approximately 5% of the measured quantity. The metal sampling was made at

irregular intervals throughout the tests, using a quartz tube which was lowered into the cathodic metal pad. The metal samples were dissolved in 10 ml concentrated HCl which was subsequently diluted with H_2O to 100 ml and analysed using an Argon ICP spectrometer. The ICP method used has a variable precision of about 10% for measured values below 100 ppm, 5% for values between 100 and 1000 ppm and 3% above 1000 ppm.

The cell was operated for 50 h with current of 25 A. The total immersed anode surface area was 75 cm^2. Current distribution calculations showed that about 40% of the current was conducted through the horizontal, bottom part of the anode, implying that the current density here was 0.8 A cm^{-2}. The cell voltage was stable during these tests with occasional disturbances associated with the metal sampling.

5. Results and discussion

During the initial stage of electrolysis, the anode material dissolves fairly rapidly until a steady state is reached. At steady state, the level of contamination is governed by the dissolution rate of the anode material and by the rate at which the species originating from the anode enter into the metal pad. Considering the mathematical treatment given above, it can be concluded that early in the test, the amount of impurities in the bath is expected to rise to the steady-state level. This rise is governed by the dissolution rate and thereby also by the mass transfer of the anode material. The concentration profile versus time can be used to calculate the time constant for the dissolution process and also the mass transfer coefficient for dissolution of the anode material. The calculation was performed by curve fitting of the concentration profile to Equation 9.

The steady-state value is a function of: (i) the solubility of the species in question, c_{sat}, (ii) the rate of reduction of the species into the cathodically deposited metal, $k_{cat}A_m$ (Equation 10) and (iii) the dissolution rate of the anode material, $k_{an}A_a(c_{sat} - c_\infty)$ (Equation 10). As the experiment proceeds, the time-dependent part of Equation 8 becomes negligible, giving a constant concentration level determined by the factor B,

$$B = \frac{k_{an}c_{sat}A_a}{k_{cat}A_m + k_{an}A_a} \qquad (11)$$

The surface ratio A_a/A_m had a value of 3 in all the experiments. As mentioned above, the mass transfer coefficient was believed to be substantially higher at the gas-evolving anode than at the cathode, leading to the assumption that B can be approximated by the total solubility of the anode species, $B = c_{sat}$.

5.1. *Dissolution of the anode material and mass transfer coefficients*

The concentrations in the electrolyte with respect to the anode components in the test with the material

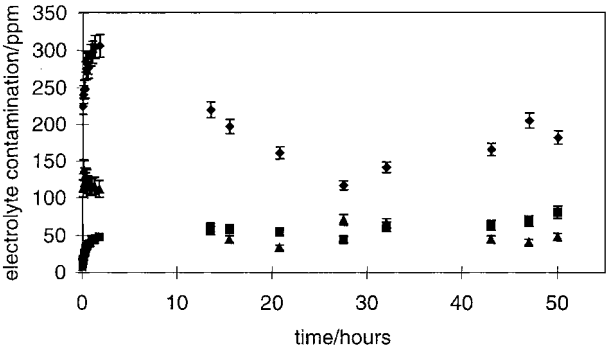

Fig. 2. Electrolyte concentration versus time for an anode with all ferrite (0% excess NiO) ceramic phase. (◆) Fe, (■) Ni, (▲) Cu.

with no excess NiO are sketched in Fig. 2. Compared to the concentration levels found in the 4-h tests, as reported in Part I [10], the Fe content found early in the 50-h tests was similar for all the materials. However, the values for Cu and Ni differed. For time less than 4 h, the concentration of Cu was considerably higher in the small cell used in [10] than in the 50-h experiments. The content of Ni was on the other hand, only slightly higher. Of these elements, only Fe was present in measurable amounts in the chemicals used to make up the electrolyte. A higher ratio of anode surface area to electrolyte volume (A_a/V) in the short-term tests may have caused this behaviour as the Ni species generally dissolved slowly while the Cu alloy metal particles on the surface of the anodes were found to dissolve more rapidly. This is also pointed out in Part I [10] where the Ni content was still rising after 4 h of electrolysis. More metal phase bleed-out on the surface of the smaller anodes used in Part I [10] may have been the reason for the higher Cu content. Care was taken to remove metallic particles from the surface of the anodes, but some may have been overlooked.

The Fe content exhibited an unexpected behaviour, as shown in Fig. 2. The initial concentration in the electrolyte was of the order of 200–300 ppm. During the first 100 min of electrolysis, the Fe content rose in a similar manner as previously observed in the 4-h tests [10], as the anode material dissolved. After this initial period, however, the Fe content fell to about one-half of what at first might have appeared to be the steady-state value. The solubility of Fe_2O_3 from nickel ferrite in cryolite at 960 °C, 6.5% Al_2O_3 and CR 2.2 (11% excess AlF_3) is reported to be about 1000 ppm [16].

In the present tests, the graphite crucible was cathodically polarized. This led to penetration of Na into the crucible material [17], effectively increasing the relative content of AlF_3. Both samples taken just before termination of the tests showed an average excess AlF_3 content of 14.6 wt% as opposed to the initial 11 wt%. This led to a marginal decrease in alumina solubility [16]. Furthermore the solubility of Fe_2O_3 has been shown to decrease somewhat with decreasing CR, going from 1200 ppm at CR = 2.6 to 1000 ppm at CR = 1.8 [16]. This change is, however,

too small to explain the observed drop from 300 to 170 ppm Fe found in Fig. 2. Another possible explanation for the curious behaviour of Fe, is the time needed to reach stable operating conditions in the cell. Although aluminium was added to the cell prior to electrolysis, stagnant layers in the bottom part of the cell may have slowed down the transfer of these species before the cell had reached stable operating conditions, as indicated by the stable contents of contaminating species in the electrolyte after about 24 h. The initial contents of Fe and Cu in the chemicals used in the electrolyte, and the content of Fe in the cell materials may account for this behaviour. After 24 h the concentrations of the anode species in the electrolyte seemed to stabilize at steady-state values. These data are summarized in Table 1.

As seen from Table 1, the steady-state values were quite similar for all the anode compositions. The concentrations in the test with the all-ferrite material (0% excess NiO) were less with respect to Ni, and the concentration of Fe was somewhat lower with the material containing most NiO. It is questionable whether these differences are significant, but it is interesting to note that they reflect the relative contents of the species in the anode materials. The solubilities of Fe_2O_3 and NiO have been investigated by De Young [16]. He determined the maximum solubilities to be 1000 and 50 ppm respectively for the given electrolyte composition and temperature. These data agree with the maximum contamination encountered after 2–3 h, but not with the steady-state values found after more than 12 h. Confidential tests performed on a different cell show the same behaviour. The Evans–Keller model (Equation 10) assumes that the dissolution of anode species into the electrolyte is much faster than the deposition of the dissolved species into the metal ($k_{an} \gg k_{cat}$). It further predicts the steady-state concentration to be close to saturation, $c_{sat} \approx c_\infty$. This does not seem to be the case, and the results suggest that the model needs to be modified.

The concentration data early in the tests were used to calculate the dissolution characteristics for the different components in the individual anodes. This was done by curve fitting of the data to the model described by Equation 9. The curves with the best fit for Ni together with the actually measured values are shown in Fig. 3.

The dissolution of Ni was very similar for all the three tested materials. After immersion of the anode into the electrolyte and start of electrolysis, the contamination of nickel in the electrolyte seemed to follow a mass transfer controlled mechanism. Curve fitting to Equation 9 described the observed dissolution well, and it is reasonable to assume a mass transfer controlled mechanism similar to the one found in the 4-h tests reported in Part I [10]. The curve fitting parameters are listed in Table 2. Compared to the parameters found in the short-term tests, the numerical values differ somewhat. The apparent, simulated steady-state concentration c_∞ is similar for all three materials, and so are the c_0 values. The c_0 values for nickel given in Table 2 are the initial concentrations estimated from the curve fitting, but the actual concentrations before anode immersion were also determined analytically by XRF for samples taken before anode immersion. These values were 7.9, and 9.4 ppm in the three experiments with the materials containing 0, 17 and 23 wt% excess NiO respectively which is close to the estimated values. In contrast to the values presented in Part I [10], the mass transfer coefficient k_{an} is almost equal for all the materials, and the values are also somewhat higher than in [10], but of the same order. Compared to the data of Weyand *et al.* [4], the present values are higher by a factor of about 2. Given the uncertainties both in the present data and those of Weyand *et al.*, finding values of approximately the same magnitude for a mass transfer controlled process is encouraging and supportive for both sets of data.

Also for Fe, the fitted curves seemed to describe the dissolution process adequately, the steady-state concentration being approximately 300 ppm. The electrolyte contained substantial amounts of Fe prior to electrolysis, as it did in the short-term tests [10].

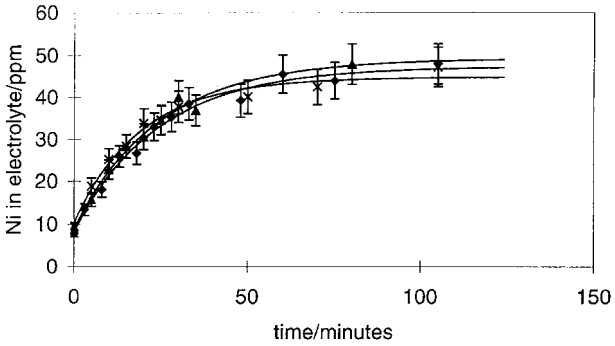

Fig. 3. Concentration of Ni in the electrolyte with the different anode materials tested versus time with best fit curves using Equation 9. (◆) 0 wt% NiO, (▲) 17 wt% NiO, (×) 23 wt% NiO.

Table 1. Steady-state values reached after 24 h for the concentrations of anode species in the electrolyte

Excess wt% NiO in material	*Fe* /ppm	*Ni* /ppm	*Cu* /ppm
0	170	60	40
17	170	80	50
23	140	80	40

CR = 1.5, 6.5 wt% Al_2O_3, 960 °C.

Table 2. Curve fitting parameters for Ni

Excess wt% NiO in material	c_∞ /ppm	c_0 /ppm	k_{an} /m s^{-1}
0	47.3	8.2	1.08×10^{-4}
17	49.2	8.9	1.92×10^{-4}
23	44.8	10.3	1.22×10^{-4}

Table 3. Curve fitting parameters for Fe

Excess wt% NiO in material	c_∞ /ppm	c_0 /ppm	k_{an} /m s^{-1}
0	309.5	227.1	8.68×10^{-5}
17	342.7	305.6	3.05×10^{-5}
23	350.8	294.4	4.93×10^{-5}

Table 4. Curve fitting parameters for Cu

Excess wt% NiO in material	c_∞ /ppm	c_0 /ppm	k_{an} /m s^{-1}
0	121.9	18.9	2.20×10^{-3}
17	247.0	7.0	1.1×10^{-3}
23*	35.7	8.1	5.49×10^{-6}

* Previously used anode.

For the three tested materials, the c_∞ and c_0 values differ more for Fe than for Ni. The two materials containing excess NiO seemed to behave quite similarly. The all-ferrite material did, however, have a higher $k_{an,\,Fe}$ value for the dissolution process. This material contains a higher proportion of nickel ferrite than the other two, and the Fe_2O_3 activity might also be higher than in the other two materials due to the possible presence of small amounts of unreacted haematite (although XRD measurements did not show any signs of Fe_2O_3), and this could be the reason for the higher dissolution rate. The somewhat lower value for the apparent steady-state concentration compared to the material with no excess NiO is difficult to explain. Compared to the results found in the 4-h tests these results are quite similar both regarding the electrolyte concentration of Fe and for the mass transfer coefficients.

The copper–nickel alloy metallic phase may exhibit a different dissolution mechanism as it did not seem to be electrochemically stable under anodic polarization in the tests reported here. Evidence suggests that the metal phase was subjected to anodic dissolution since no copper oxides were found on the surface of the anodes after electrolysis. Tarcy [12] suggested that while Ni was subject to anodic dissolution, a stable oxide layer would form on Cu in the cermet during electrolysis. As already stated, copper oxides may form, but XRD measurements did not show any copper oxides to be present within the sensitivity of that method [14]. The model used here may not describe the electrochemical process very well as it is based on the assumption of a simple chemical dissolution mechanism, and the concept of a chemical mass transfer coefficient $k_{an,\,Cu}$ for copper is therefore of doubtful significance.

The behaviour with respect to copper of the material containing 23 wt% NiO was interesting, as it differed strongly from the other two. Much lower values both for the steady-state contamination and for the mass transfer coefficient were found. This particular anode had been used in a failed experiment prior to the experiment described here (the experiment was terminated due to crucible failure). The anode surface was, therefore, probably depleted of metallic phase prior to this experiment. The concentration of Cu in the electrolyte in all the experiments eventually approached a level of around 40–50 ppm. A possible explanation is that the metal-rich surface of the anodes dissolved rapidly until a stable Ni-Fe_2O_4–NiO boundary layer was formed. The values obtained with an already used anode should, therefore, give more correct data for the real steady-state Cu concentration in the experiments. The total amount of copper dissolved initially from new anodes was of the order of 0.4 g, based on a maximum concentration of 200 ppm in the electrolyte. This is a significant amount, which should be taken into account when considering the contamination of the deposited metal.

The Cu dissolution rate found for the pre-electrolysed anode was very low. This may describe the actual wear of the anode in that the mechanism at steady state, is, anodic dissolution of the metal particles, exposed to electrolyte as the metal depleted ferrite-oxide layer recedes as the oxides dissolve. The relative amounts of anode constituents reduced to metal did not, however, reflect the composition of the anode material. Ray [25] and Weyand *et al*. [4] tested cermet anodes with varying metal phase contents. The best results (lowest corrosion) were obtained with an anode material similar to that containing 17 wt% excess NiO in this study. The relative amounts of anode constituents found are somewhat closer to the ratios in the anode than those reported by Ray, but in general the same trends are found; that substantially more iron and copper than nickel are reduced to metal than can be explained by uniform dissolution of the anode material. This may be attributed to different transfer characteristics for the various species into the vapour phase or deposition of nickel-containing compounds elsewhere, i.e. on the alumina liner as nickel aluminate, although this was not observed in post-mortem examination of the cell. For further investigations with these materials, it is recommendable to pre-electrolyse the substrates to achieve a metal-free, stable surface, and to collect samples of condensed vapour to determine the amount of anode constituents leaving the cell via the vapour phase. Impurities may also originate from other sources, ie. the electrolyte itself, the crucible, or the alumina fed to the cell during electrolysis.

5.2. *Metal contamination and transfer of impurities*

The contents of anode components in the deposited metal for the anode with no excess NiO are shown in Fig. 4. The material containing no excess NiO showed an increase in contamination early in the experiment, but the concentrations stabilized after 20–24 h of electrolysis. For the other two materials, it took a longer time for the contamination to reach a steady level, especially for the material containing 23 wt% NiO. In this experiment, the concentration of

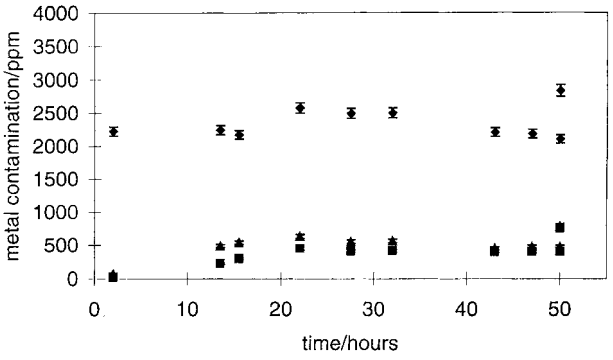

Fig. 4. Metal contamination of anode constituents versus time. The anode contained no excess NiO. The higher values at 50 h represent the contamination in metal samples taken after solidification. (◆) Fe; (■) Ni; (▲) Cu.

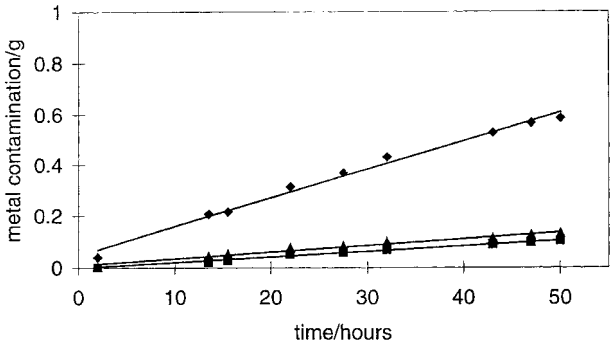

Fig. 5. Transfer of anode species into the metal vs time. The anode contained no excess NiO. The lines drawn represent linear behaviour. (◆) Fe; (■) Ni; (▲) Cu.

Ni in the metal was still rising after 50 h of electrolysis. A common feature for all the materials was that copper seemed to enter the deposited metal more rapidly than nickel. This agrees with the measurements of impurities in the electrolyte where Cu quickly entered the electrolyte, while the NiO dissolved more slowly. The metal contamination obtained with the materials tested in this study is in the same range as that found by Ray for a material containing 18 wt% excess NiO [18].

The results with the material containing no excess NiO were especially encouraging. Contents of 2200 ppm Fe, 400 ppm Ni and 400 ppm Cu gave a total contamination of 2800 ppm. Overall, this gives acceptable purity as primary metal although the contamination of Ni and Cu is above specifications. It was also encouraging to see that the contamination reached a steady state, suggesting that this was the actual contamination caused by the anode material corroding in a controlled manner together with the effect of iron impurities coming from other sources. Also the material containing 17 wt% excess NiO seemed to reach such a steady state albeit after a longer period of electrolysis. For this anode material, the contamination of the deposited metal was higher for all the species, implying a higher overall corrosion rate. In the experiment with the all-ferrite material (0% excess NiO), the amount of anode constituents in the metal was also measured after the cell had cooled and the metal pad had solidified. As can be seen in Fig. 4, substantial amounts of contaminants entered the metal after electrolysis was terminated.

If the anode materials dissolve at a constant rate, the quantity of dissolved material ending up in the metal should increase linearly with time, provided the concentration in the electrolyte remains constant. The amounts of material which entered the aluminium cathode in the test with the all-ferrite material (0 wt% excess NiO) are plotted in Fig. 5. The figure show the total amounts of anode species in grams of metal having entered the deposited metal. The contents of anode species in the electrolyte are not included because they reached steady state, and hence did not contribute to the time-dependent corrosion. A linear process was assumed, so the curves in the figure are fitted to a simple linear equation (Equation 10). Losses to the vapour phase where not considered, as this amount was not known, because of the unknown transfer characteristics into the vapour phase. All the materials showed a linear behaviour with respect to anode species entering the deposited metal.

Due to a computational error, previously published data for the contamination of the metal, the mass transfer coefficients for the anode corrosion products entering the metal and the anode corrosion rates were too low by a factor of 10 [19].

The amounts of anode constituents which entered the metal were clearly linear with time as demonstrated by the straight lines in Fig. 5. This observation suggests that the anodes dissolve at a constant rate. The extrapolated corrosion rates in cm per year of operation calculated from the linear behaviour was 1.2, 1.7 and 2.0 cm $year^{-1}$ for the three materials, respectively. The two materials, containing excess NiO showed very similar characteristics with regard to the transfer of species into the metal, while the all-ferrite material showed considerably lower values. The numerical values of the mass transfer coefficients are listed in Table 6.

Table 5. Quantities of anode species which entered the metal in the tests with cermet anodes of different compositions

Material	*Fe* /g s^{-1}	*Ni* /g s^{-1}	*Cu* /g s^{-1}
0 wt% NiO	3.11×10^{-6}	0.58×10^{-6}	0.70×10^{-6}
17 wt% NiO	6.92×10^{-6}	1.29×10^{-6}	1.84×10^{-6}
23 wt% NiO	5.58×10^{-6}	1.49×10^{-6}	1.31×10^{-6}

A linear process was assumed.

Table 6. Mass transfer coefficients for the different anode species which entered the deposited metal

Material	$k_{cat,Fe}$ /m s^{-1}	$k_{cat,Ni}$ /m s^{-1}	$k_{cat,Cu}$ /m s^{-1}
0 wt% NiO	2.99×10^{-6}	1.59×10^{-6}	2.86×10^{-6}
17 wt% NiO	6.65×10^{-6}	2.64×10^{-6}	6.00×10^{-6}
23 wt% NiO	6.52×10^{-6}	3.04×10^{-6}	5.34×10^{-6}

The values in Tables 1 and 5 were used together with Equation 10.

Again, the all-ferrite material differed markedly from the two others which were similar. This behaviour is difficult to explain for a mass transfer controlled process because the mass transfer coefficient for a given species should be the same for all the anode materials. A possible explanation might be that, at the temperatures used in these experiments, the all-ferrite material (no excess NiO) had a significantly lower electrical conductivity than the two materials containing excess NiO [10]. The lower conductivity led to higher cell voltage and forced more current to pass through the upper parts of the sidewall of the anode, giving less gas evolution around the bottom of the anode and possibly, thereby, a thicker diffusion layer at the metal pad at the bottom of the cell. A doubling of the diffusion layer thickness is sufficient to explain the observed behaviour. After the tests the cells were cut into halves and a distinct layer was evident above the cathode. This layer seemed to be more compact than the rest of the electrolyte, suggesting that the electrolyte in this layer was super-saturated with respect to alumina. Chin [20], found that a Cu-rich "skim layer" was formed above the polarized metal. In that study, copper, nickel and iron were dissolved in the form of oxides from sintered tablets and the subsequent transfer of the species from the electrolyte into the metal was studied. Such a "skim" layer was not observed in the present study.

Table 7 gives the ratios between the mass transfer coefficients for the anode species having entered the metal. These numbers should cancel out the effect of diffusion layers of unequal thickness and reflect the ratios between the diffusion coefficients. The numbers match fairly well and suggest that Fe and Cu had approximately the same characteristics, iron being slightly more mobile than Cu. It is interesting to note that Ni entered the metal pad at about half the rate of Fe and Cu. This observation suggests that an anode material based on Ni, be it nickel oxide or some other nickel compound, has the most promising potential for an inert anode material. If a NiO-based material can be made with adequate electrical conductivity, it should be investigated further.

5.3. *Material performance*

SEM pictures of cross-sections of the anode surfaces are shown in Fig. 6. The materials seemed to be very stable as there were no visible structural changes when going from the unchanged interior of the electrode to the surface. On all anodes a distinct layer of about 50 μm thickness had been formed at the surface. A similar layer of about 20 μm thickness was observed in the 4-h short-term experiments [10]. The layer formed on the material containing no excess NiO was dense compared to the interior of the anode, which contained some pores. The porosity was attributed to the poorer sintering characteristics of this material [10]. Since the surface layer of this anode is more dense than the anode material itself, the layer may have formed via a reaction forming aluminates such as $FeAl_2O_4$, which has been detected by XRD [14]. The formation of the surface layer is clearly not just the result of the dissolution of the metal grains exposed to the electrolyte leaving the ferrite matrix behind.

Table 7. The ratios between the different mass transfer coefficients

Material	$k_{cat,Fe}/k_{cat,Ni}$	$k_{cat,Fe}/k_{cat,Cu}$	$k_{cat,Cu}/k_{cat,Ni}$
0 wt% NiO	1.88	1.05	1.80
17 wt% NiO	2.52	1.11	2.27
23 wt% NiO	2.14	1.22	1.76

Polished samples were analysed by X-ray microanalysis (XRMA) with an energy dispersive spectrometer connected to the SEM. Quantitative chemical analyses were performed on the different phases in the anodes in three positions relative to the anode–electrolyte interface, i.e. (i) in the interior (>2 cm from the interface), (ii) 200 μm from the interface and (iii) immediately below the 50 μm thick reaction layer which had formed on the surface. The data for the metal phase are given in Table 8. The reaction layer was also analysed by the same method, and data are given in Table 9. The equipment was fitted with a Be window which excluded analysis of light elements such as oxygen, and the results were therefore normalized to 100% with respect to the metal cations.

The XRMA analyses showed that the oxide phases in the cermets were stable with regard to composition during electrolysis, as the relative amounts of Ni and Fe did not change from the interior of the anode to the outer surface. Variation in the oxygen content could, as mentioned earlier, not be studied. The metallic phase was systematically depleted with respect to Ni in the alloy when going from the interior to the surface of the cermets. The surface layer contained minor amounts of Al, suggesting that small amounts of aluminates were formed, as also observed in earlier work [14]. Sadoway [26] sets as a criterion for an inert anode material, that the material is not attacked by aluminium dissolved in the melt. If aluminium should reach the cermet anode surface it may undergo aluminothermic reduction.

The source of aluminium found in the reaction layer in the present work was probably alumina, being much more likely than dissolved aluminium reaching the anode which is surrounded by oxygen bubbles. If this is the case, the assumption that the anode corrosion process is governed purely by a mass transfer controlled process due to chemical dissolution, might be wrong. If a chemical reaction, such as the formation of aluminates, takes place on the surface of the cermet, this may have serious implications in the understanding of the behaviour of oxide-based anodes in cryolitic melts. McLeod *et al.* [27] studied the reaction zone on a single crystal cobalt ferrite sample used as anode in an alumina-saturated cryolite melt at 960 °C and found a reaction layer of about

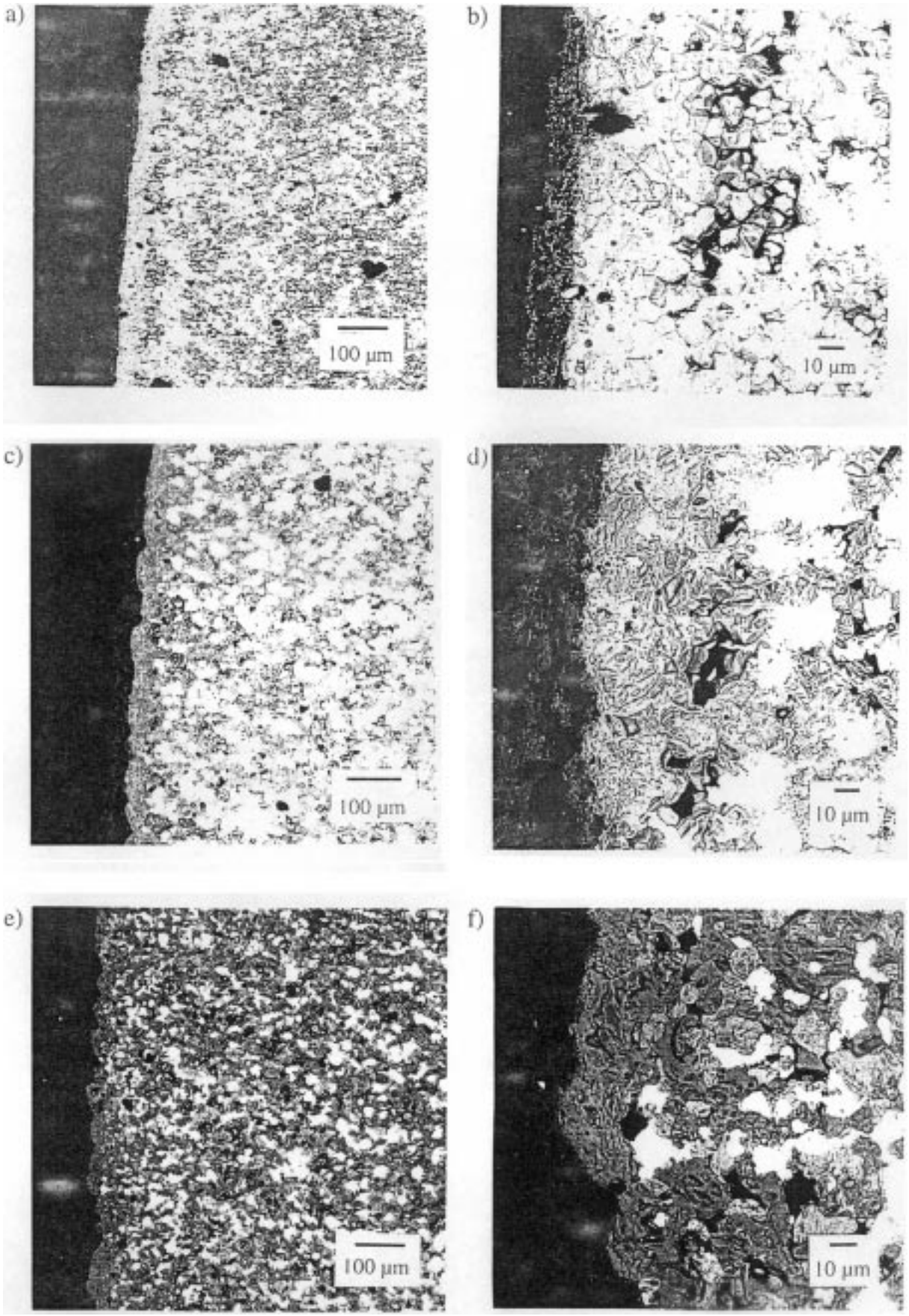

Fig. 6. SEM micrographs of cross-sections of the cermet–electrolyte boundary of anodes after 50 h of electrolysis. (a) 0% excess NiO; (b) as (a), but higher magnification; (c) 17% excess NiO; (d) as (c) but higher magnification; (e) 23% excess NiO; (f) as (e), but higher magnification.

Table 8. XRMA analyses of the metal in different parts of the anode samples

Excess wt% NiO in material	*Position relative to interface*	*Al* /rel. at%	*Fe* /rel. at%	*Ni* /rel. at%	*Cu* /rel. at%
0	Interior	0	8.4 ± 0.2	38.8 ± 0.5	52.1 ± 0.7
	200 μm	1.1 ± 0.2	7.6 ± 0.2	24.2 ± 0.4	67.0 ± 0.8
	20 μm	1.0 ± 0.1	5.2 ± 0.2	22.4 ± 0.4	71.3 ± 0.8
17	Interior	0	5.0 ± 0.2	39.8 ± 0.6	56.6 ± 0.8
	200 μm	0	3.7 ± 0.2	22.7 ± 0.5	73.4 ± 0.9
	20 μm	0	4.2 ± 0.2	20.6 ± 0.5	75.1 ± 0.9
23	Interior	0	2.1 ± 0.1	36.0 ± 0.5	61.4 ± 0.7
	200 μm	0	3.8 ± 0.2	21.0 ± 0.5	75.2 ± 0.9
	20 μm	0	5.0 ± 0.2	21.5 ± 0.4	73.6 ± 0.9

Rel. at% relates to the results being normalized to 100% for all the species analysed (see text).

Table 9. XRMA analyses of the outer 50 μm surface layer facing the anode–electrolyte interface for the different anode samples

Excess wt% NiO in material	*Al* /rel. at%	*Fe* /rel. at%	*Ni* /rel. at%	*Cu* /rel. at%
0	2.9 ± 0.1	67.9 ± 0.9	25.6 ± 0.4	4.5 ± 0.3
17	2.5 ± 0.2	68.2 ± 0.5	27.1 ± 0.5	2.1 ± 0.3
23	1.3 ± 0.1	68.5 ± 0.6	29.6 ± 0.5	0.6 ± 0.2

8 μm thickness which contained considerable amounts of aluminium which they suggested was alumina in solid solution with the cobalt ferrite. This may have been in the form of a separate phase of aluminates.

The solubility of oxides in cryolitic melts is very dependent on the content of alumina. De Young [16] reports the solubility of NiO in a melt with CR 2.2 at 960 °C to be about 1000 ppm as Ni at 2.5 wt% Al_2O_3. At 6.5 wt% Al_2O_3, the Ni solubility had dropped to about 200 ppm. To exhibit a slow dissolution rate into the electrolyte for oxidic anodes, it is necessary to keep the alumina content in the electrolyte fairly high. In commercial cells today, the alumina content in the electrolyte is maintained at a value in the range 2–4 wt%. If oxidic anodes are to be utilized, a new type of process control where the alumina content in the electrolyte can be kept at a higher level is needed. One such process has recently been patented by Beck [28] of use with metallic anodes by maintaining alumina in suspension in the electrolyte.

Acknowledgements

The authors gratefully acknowledge financial support from the Norwegian aluminium industry and the Norwegian Research Council. This work was conducted in partial fulfilment of the requirements for a dr.ing. (Ph.D.) degree.

References

[1] H. Alder, US Pat. 3.960.678 (1976).
[2] V. deNora, P. M. Spaziante and A. Nidola, US Pat. 4.098.669 (1978).
[3] K. Yamada, T. Hashimoto and K. Horinouchi, UK Pat. 1.146.155 (1977).
[4] J. D. Weyand, D. H. DeYoung, S. P. Ray, G. P. Tarcy and F. W. Baker, 'Inert Anodes for Aluminium Smelting, Final Report', Aluminium Company of America, Alcoa Laboratories, Alcoa Center, DOE/CS/40158-20, Idaho Operation Office, Idaho Falls, ID (1986).
[5] C. F. Windisch and S. C. Marschman, 'Electrochemical Polarization Studies on Cu and Cu-containing Cermet Anodes for the Aluminium Industry', Battelle-PNL report No. PNL-SA-14299, Pacific Northwest Laboratories, Richland, WA, USA (1986).
[6] C. F. Windisch, *J. Electrochem. Soc.* **138** (1991) 2027.
[7] C. F. Windisch and N. D. Stice, 'Report on the Source of the Electrochemical Impedance on Cermet Inert Anodes', Battelle-PNL report No. PNL-7629, Pacific Northwest Laboratories, Richland, WA, USA (1991).
[8] C. F. Windisch and N. D. Stice, 'Final Report on the Characterization of the Film on Inert Anodes', Battelle-PNL report No. PNL-7589, Pacific Northwest Laboratory, Richland, WA, USA (1991).
[9] C. F. Windisch and N. D. Stice, 'Laboratory-Scale Testing of Non-Consumable Anode Materials', Battelle Pacific Northwest Laboratories, Richland, WA, PNL-6805 (1989).
[10] E. Olsen and J. Thonstad, 'Nickel ferrite as inert anodes in aluminium electrolysis: Part I Material fabrication and preliminary testing', *J. Applied Electrochem* **29** (1999) 293–299.
[11] E. Olsen, 'Nickel Ferrite and Tin Oxide as Anode Materials for Aluminium Production', Dr. Ing. thesis, University of Trondheim, Trondheim, Norway (1995).
[12] G. P. Tarcy, Conference paper, Light Metals 1986, (edited by R. E. Miller), the Minerals Metals and Materials Soc., Warrendale, PA (1986) pp. 309–320.
[13] C. M. Hall, US patent No. 400.766 (1889).
[14] E. Olsen, Graduation thesis, Norwegian Inst. of Technology (1991).
[15] J. W. Evans and R. Keller, 'Factors Affecting the Life Time of Inert anodes for Aluminum Electrolysis', Electrochem. Soc. meeting Extended abstract No. 653, Pennington, NJ, (1986) p. 966.
[16] J. D. DeYoung, Conference paper, Light Metals 1986 (edited by R. E. Miller), The Minerals Metals and Materials Soc., Warrendale, PA (1986) pp. 209–309.
[17] M. Sørlie and H. A. Øye, 'Cathodes in Aluminium Electrolysis', 2nd edn, Aluminium-Verlag, Düsseldorf (1994).

[18] S. P. Ray, Conference paper, Light Metals 1986 (edited by R. E. Miller), The Minerals Metals and Materials Soc., Warrendale, PA (1986) pp. 287–298.
[19] E. Olsen and J. Thonstad, Conference paper, Light Metals 1996 (edited by W. Hale), The Minerals, Metals and Materials Soc., Warrendale, PA (1996) pp. 249–258.
[20] P. C. Chin, 'The behavior of impurity species in Hall-Heroult aluminum cells', Ph.D. Thesis, Carnegie Mellon University, Pittsburgh, PA, USA (1992).
[21] D. H. Zöllner and H. Hahn, Öfenlegungsschrift DE 3537575 Al, 22 Oct (1995).
[22] H. Alder, Us patent 3.960.678 (1976).
[23] K. Yamada, T. Hashimoto and K. Horinouchi, UK patent 1.146.155 (1977).
[24] H. Alder, US patent 4.357.226 (1982).
[25] K. Horinouchi, N. Tahikawa and K. Yamada, Proceedings of the first international symposium on Molten Salt Chem. and Techn., Kyoto (1983) p. 66
[26] D. R. Sadoway, Conference paper, Light Metals 1990 (edited by C. M. Bickert), The Minerals, Metals and Materials Soc., Warrendale, PA (1990) pp. 403–407.
[27] A. D. McLeod, J-M Lihrmann, J. S. Haggarty and D. R. Sadoway, Light Metals 1987, The Minerals, Metals and Materials Soc., Warrendale, PA (1987) pp 357–365.
[28] T. R. Beck and R. J. Brooks, US patent 5.006.209
[29] J. N. Hryn and D. R. Sadoway, Light Metals 1993, The Minerals, Metals and Materials Soc., Warrendale, PA (1993) pp. 475–483.
[30] C. Zöllner, 'Dimensionsstabile Elektroden für die Schmelzflusselektrolyse', Berichtsnummer BMFT-FB-T 85 186, Bundesministerium für Forscung und Technologie, Bonn, Germany (1985).
[31] H. Zhang, V. De Nora and J. A. Sekhar, 'Materials Used in the Hall-Heroult Cell for Aluminium Production', The Minerals Metals and Materials Soc., Warrendale, PA (1994).
[32] A. I. Belyaev and A. E. Studentsov, *Legkie Metally* **6**(3) (1937) 17.
[33] A. I. Belyaev and A. E. Studentsov, *Legkie Metally* **8**(1) (1938) 7.